# Evaporation of Sessile Droplets on Slippery Liquid-Infused Porous Surfaces (SLIPS)

Jian H. Guan, Gary G.Wells,* Ben Xu and Glen McHale

*Smart Materials and Surfaces Laboratory*, Department of Physics & Electrical Engineering, Northumbria University Newcastle, Ellison Place, Newcastle upon Tyne, NE1 8ST, United Kingdom

David Wood

Microsystems Technology Group, School of Engineering and Computing Sciences, Durham University, South Road, Durham, DH1 3LE, United Kingdom

James Martin and Simone Stuart-Cole

Reece Innovation, Newcastle upon Tyne, NE6 3QS, United Kingdom

## ABSTRACT

Over the last decade the most common approach to creating liquid shedding surfaces has been to amplify the effects of non-wetting surface chemistry, using micro/nano-texturing to create superhydrophobic and superoleophobic surfaces. Recently, an alternative approach using impregnation of micro/nano-textured surfaces with immiscible lubricating liquids to create slippery liquid-infused porous surfaces (SLIPS) has been developed. These types of surfaces open up new opportunities to study the mechanism of evaporation of sessile droplets in zero contact angle hysteresis situations where the contact line is completely mobile. In this study, we fabricated surfaces consisting of square pillars (10 – 90μm) of SU-8 photoresist arranged in square lattice patterns with the centre-to-centre separation between pillars of 100μm, on which a hydrophobic coating was deposited and the textures impregnated by a lubricating silicone oil. These surfaces showed generally low sliding angles of $1^{o}$ or less for small droplets of water. Droplet profiles were more complicated than on non-impregnated surfaces and displayed a spherical cap shape modified by a wetting ridge close to the contact line due to balancing the

interfacial forces at the line of contact between the droplet, the lubricant liquid and air (represented by a Neumann triangle). The wetting ridge leads to the concept of a wetting "skirt" of lubricant around the base of the droplet. For the SLIPS surfaces we found that the evaporation of small sessile droplets (~2 mm in diameter) followed an ideal constant contact angle mode where the apparent contact angle was defined from the intersection of the substrate profile with the droplet spherical cap profile. A theoretical model based on diffusion controlled evaporation was able to predict a linear dependence in time for the square of the apparent contact radius. The experimental data was in excellent quantitative agreement with the theory and enabled estimates of the diffusion constant to be obtained.

## 1. INTRODUCTION

Liquid evaporation is a wide spread phenomenon and can be seen in natural processes such as rain, snow formation, dew and fog[1]. Liquid evaporates if the surrounding atmosphere is not saturated with the vapour of the droplet's liquid. However, evaporation may occur in saturated conditions if the size of droplets is very small due to an increase in vapour pressure caused by the surface curvature of the droplet. Free evaporation of small and spherical droplets of water has attracted extensive attention due to its widespread relevance to engineering applications such as ink-jet printing[2], thin film coatings[3], automatic DNA mapping[4] and spraying of pesticides[5]. These applications often involve small droplets deposited on solid substrates and having sizes below the capillary length such that the drop shape is dominated by surface tension rather than gravity.

A foundational study of sessile drop evaporation was carried out by Picknett and Bexon[6] in which they considered the theory for diffusion controlled evaporation and experimentally

observed the mass and profile evolution of slowly evaporating droplets on a Teflon surface in air. They pointed out that when a completely spherical drop on a solid substrate has a contact angle of 180° its evaporation rate is lower than that of an equivalent volume hanging spherical drop in free space due to the reduced space into which the liquid may diffuse. An exact equation for the rate of mass loss in this situation was derived by Picknett and Bexon[6] by using the analogy between the diffusive flux and the electrostatic potential, and it was found to be valid for droplets resting on a solid boundary with a spherical cap shape. In this study, three possible modes of evaporation were reported: i) constant contact angle with diminishing contact area, ii) constant contact area with diminishing contact angle, and iii) a mixed mode with changes in both the contact area and contact angle. Recent reviews of sessile droplet evaporation include those by Cazabat & Guéna[7], Erbil[1] and Larson[8]. Most recently, Stauber *et al.* have theoretically considered the evaporation of droplets on strongly hydrophobic substrates with a focus on the constant contact radius and constant contact angle modes[9].

In one of the earliest studies, Birdi and Vu[10] reported the constant contact area mode of evaporation in their investigation of the evaporation rate of sessile droplets of water placed on a smooth solid surface and in which they observed a constant radius of the liquid-solid interface and a decrease in the contact angle. In their subsequent work[11], the effect of wetting characteristics on the rate of evaporation of droplets of liquids was demonstrated. It was shown that water on glass with a contact angle < 90° evaporated in constant contact area mode; whereas water on Teflon with a contact angle of > 90° evaporated with a constant contact angle and a diminishing contact area. Shanahan and Bourgès[12] also considered the evaporation of water droplets with contact angles below 90° from both smooth and rough surfaces and obtained measurements of the change in contact angle, drop height and contact radius with time. Rowan *et*

*al.* demonstrated in two separate studies[13, 14], the change of contact angle with time via detailed measurements of various geometrical parameters on systems with $\theta < 90°$ and gave a theoretical model based on a diffusion model suggested by Birdi *et al.*[10]. They later presented detailed measurements for evaporation of sessile drops in a system with $\theta > 90°$ in which they showed that the evaporation is dominated by an initial stage with constant contact angle and a diminishing contact radius[15].

Despite extensive research, obtaining experimental systems that are close to a constant contact angle mode for evaporating sessile droplets remains difficult due to contact angle hysteresis. Smooth solid surfaces tend to have significant contact angle hysteresis and so as a droplet evaporates the contact line is often pinned and will then recede in a stepwise fashion. Due to their water shedding ability superhydrophobic surfaces are often referred to as "slippery" when demonstrating a Cassie-Baxter state[16], thus making them candidates for studying the constant contact angle mode. McHale *et al.* were the first to report the evaporation of sessile water droplets on lithographically fabricated superhydrophobic surfaces[17]. They observed a brief initial constant contact area period, followed by a de-pinning which displayed a step-wise retreat of the contact line, reflecting the periodicity of the underlying surface texture. In some cases, a collapse of the droplet into the surface texture occurred during the later stages of evaporation displaying a transition to a "sticky" Wenzel state[18], which resulted in a completely pinned droplet[17, 19, 20, 21]. Many studies have since looked into the evaporation of droplets on superhydrophobic surfaces[19, 20, 21, 22, 23, 24], but studying the evaporation of water droplets on surfaces with low contact angle hysteresis remains challenging.

Recently, new types of surfaces, Slippery Liquid-Infused Porous Surfaces (SLIPS), inspired by the Nepenthes pitcher plant, have been developed[25]. These exhibit excellent non-wetting

performances and provide an alternative to traditional superhydrophobic surfaces[26, 27, 28, 29, 30]. SLIPS surfaces employ micro/nano-texture to facilitate the wicking of a non-volatile lubricating liquid which is immiscible to the sessile droplet. These surfaces show low sliding angles[26, 27, 28, 29, 30], self-healing properties through capillary wicking upon damage[28], have anti-icing abilities[31] and are capable of withstanding external pressure[28]. Several thermodynamically stable states can exist when a droplet is placed on a SLIPS surface depending on the spreading coefficient of the lubricating liquid and the test liquid as well as the surface texture[26]. These relate to whether the lubricant not only fills the texture, but whether it also exists as a film above the surface features both under the droplet and external to the droplet[26]. The most slippery states correspond to the case whereby a lubricating layer is present as a continuous layer between a droplet and the solid substrate beneath. One further complication is whether the surface energetics favours the spreading of a thin layer of the lubricant completely across the liquid-vapour interface of the sessile droplet[26].

The development of SLIPS surfaces offers an opportunity to study the evaporation of droplets of water with highly mobile contact lines not subject to the contact line pinning of previous surfaces. However, it also touches upon fundamental questions relating to wetting and interpretation of contact angles. When a droplet is deposited on a rigid solid substrate it forms a sessile droplet and its contact angle is described in an idealised concept using Young's law; on real surfaces contact angle hysteresis is an experimental fact. When a droplet is deposited on a liquid sub-phase it forms a liquid lens and the three-phase contact line between the droplet, the liquid subphase and the air is determined by a balance of interfacial forces often depicted pictorially using a Neumann's triangle. In between these two cases is the case whereby a droplet is deposited on a soft surface and the vertical component of the droplet's surface tension deforms

the surface and creates a wetting ridge. In the case of a droplet deposited on a SLIPS surface their appears to be a sessile droplet rather than a liquid lens, but because the sdroplet rests on a layer of liquid lubricant the region close to the solid surface shows a more complex shape with a wetting ridge due to the balance interfacial forces at the line of contact between the droplet, lubricant liquid and air, as shown in Figure 1a. The lack of direct contact of the sessile droplet with the underlying solid surface makes it less clear how a contact angle might be defined and how previous theories, which included droplet-solid contact angle and contact area, may relate to the evaporation process. Compared to "slippery" superhydrophobic surfaces, which involve the sessile droplet bridging across air gaps between features, a transition to a "sticky" Wenzel state might not be anticipated when lubricant already fills the gaps between surface features.

Here we present an experimental study in which we used SLIPS surfaces to create a system with an apparent contact angle greater than 90°, and where droplets of water are highly mobile with very low contact angle hysteresis. We also develop a theoretical model to estimate the diffusion coefficient based on a previous diffusion limited evaporation model modified to use apparent contact angles and contact areas and to account for the presence of a wetting skirt created by the interfacial forces at the line of contact between the lubricating liquid, the evaporating droplet and the surrounding air. Thus, we report a paradoxical situation where we study an apparent constant contact angle mode of sessile droplet evaporation, but where the droplet is deposited on a layer of lubricant liquid rather than into direct contact with the solid. Despite that paradox, it proves possible to describe the process using all the machinery and tools developed for sessile droplet evaporation on solid surfaces providing the wetting ridge is accounted for using the concept of a wetting skirt and care is taken in defining apparent contact angles and contact radii.

## 2. THEORETICAL DEVELOPMENT

### *2.1 Model Fundamentals*

The surfaces in our studies use a textured solid surface into which a non-volatile lubricant liquid has been impregnated. The solid texture locks in the lubricant, which is chosen to also coat the tops of the solid texture so that there is a continuous layer of liquid lubricant. Despite the fact that the droplet is deposited onto a layer of liquid rather than into direct contact with the solid, the majority of its shape is described as a section of a spherical cap in the same manner as a sessile droplet resting on a solid surface. The use of a SLIPS surface means that there is no longer a Young's law contact angle at a liquid-solid-vapour three-phase contact line, but there is force balance between three interfacial tensions at the line of contact between the droplet, the lubricant liquid and air (described by a Neumann force triangle), which results in a wetting ridge.

In previous studies of evaporation of sessile droplets the droplet shape and volume was determined using measurements of the contact angle and the contact or spherical radius of the droplet. However, as Figure 1a shows, on a SLIPS surface defining and extracting a contact angle at the edge of the droplet is no longer a simple concept. At the intersection between the infusing liquid, the water and the surrounding air, the three interfacial forces balance (often represented by a Neumann triangle) at the base of the droplet lead to a wetting ridge around the droplet. The height of the ridge around the droplet can be significant with respect to the overall height of the droplet and the evaporation surface area, and therefore hinders evaporation of the droplet at its base. This effect of a wetting ridge creating a lubricant skirt around the base of the droplet must be taken into account in developing any model to describe the evaporation; using a dye to dope the water droplet we confirmed that the liquid within the skirt was lubricant.

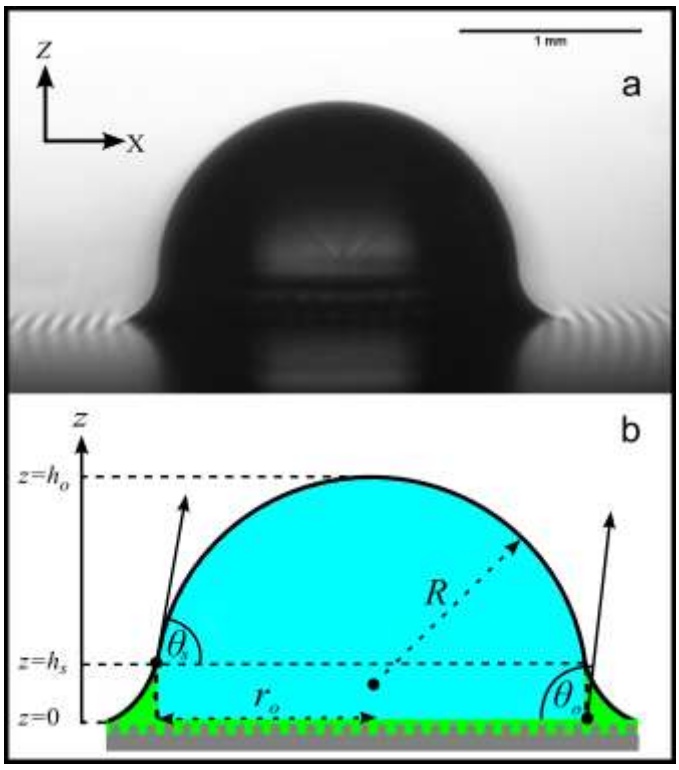


Figure 1: a) Image of a sessile droplet of water on a SLIPS surface showing a wetting ridge formed by the balance of forces between the non-evaporating lubricating liquid and the evaporating droplet. b) Cross section schematic of the droplet on a lubricant impregnated textured surface showing defined parameters and a wetting skirt of non-volatile lubricant created by the wetting ridge.

Figure 1a shows that because the droplet size is much less than the capillary length of the evaporating liquid, $\kappa^{-1}=(\gamma_{LV}/\rho g)^{1/2}$, where $\gamma_{LV}$ is the surface tension, $\rho$ is the density of the liquid and $g$ is the acceleration due to gravity, the assumption that the droplet adopts a spherical cap shape remains valid away from the surface. For a given volume of liquid, there are therefore well-defined geometric parameters which can be measured from side profile images. These include the spherical radius $R$, apparent contact radius $r_o$, apparent contact angle $\theta_o$ and the apex height $h_o$, above the contact surface (Figure 1b). In analysing an image of a spherical cap with a given spherical radius using a side profile view, the vertical placement, in the $z$ direction, of the position of the contact surface alters the deduced volume, $V(z)$, apparent contact radius $r(z)$,

apparent contact angle $\theta(z)$ and apex height $h(z)$ and is therefore an important consideration. Geometrically, these parameters are related by,

$$r(z) = R\sin\theta(z) \tag{1}$$

and

$$V(z) = \frac{\pi\beta(\theta)R^3}{3} \tag{2}$$

where

$$\beta(\theta) = 2 - 3\cos\theta(z) + \cos^3\theta(z) = (1-\cos\theta(z))^2(2+\cos\theta(z)) \tag{3}$$

The apex height measured from the position $z$ is given by,

$$h(z) = R(1-\cos\theta(z)) \tag{4}$$

In general, the rate for diffusion limited loss of a liquid volume by evaporation through a liquid-vapour interface is,

$$\frac{dV}{dt} = -\frac{D}{\rho}\int \underline{\nabla C}.\underline{dS} \tag{5}$$

where $D$ is the diffusion coefficient of the vapour and $\rho$ is the density of the liquid[6]. Combining the geometrical assumptions with eq. (5) and a concentration gradient model allows data on the evaporation of sessile droplets to be analysed.

### *2.2 General Model for Diffusion-Limited Evaporation from SLIPS Surfaces*

In previous work on evaporation of sessile droplets in a constant contact angle mode Erbil[32] introduced a function $f(\theta)$ to take account in a common notational format of the dependence of

the concentration gradient of vapour, between the surface of the droplet and its surroundings, on the contact angle arising from different models: a notation which was also used in studies of droplet evaporation from superhydrophobic surfaces.[17] In this notation, eq. (5) becomes,

$$\frac{dV}{dt} = -2\lambda R f(\theta) \tag{6}$$

One simple approach used in the literature[13], has been to approximate the concentration gradient to be radially outward and equal to $(c_s\text{-}c_\infty)/R$, where $(c_s\text{-}c_\infty)$ is the difference in the vapour concentration at the liquid-vapour interface of the droplet $c_s$, which is assumed to be its saturation value, and that far removed from the droplet surface $c_\infty$, which is assumed to be its ambient value.[13] This approximation to the concentration gradient is intuitive and accurate for contact angles close to $90^o$, but ignores the contact angle dependence that is introduced by the presence of the substrate which restricts the space into which vapour can diffuse. With this approximation the function, $f(\theta)$, becomes,

$$f_R(\theta) = \frac{1-\cos\theta}{2} \tag{6}$$

and eq. (5) gives the evaporation rate to be,

$$\frac{dV}{dt} = -\lambda h_0 \tag{7}$$

where $\lambda = 2\pi D(c_s\text{-}c_\infty)/\rho$ and $h_o = h\ (z = 0)$.

In the case of the droplet on a SLIPS surface the "skirt" of lubricating liquid that rises to a height $h_s$, above the surface structure, reduces the droplet's liquid-vapour interfacial area, by masking the bottom of the droplet with a layer of the non-volatile lubricating liquid (Figure 1b).

The liquid-vapour surface area through which evaporation occurs is therefore modified and results in the modified evaporation rate of the droplet,

$$\frac{dV}{dt} = -\lambda h_o \left[ 1 - \frac{h_s}{h_o} \right] \tag{8}$$

The existence of a skirt of impregnating (lubricant) liquid around the base of the droplet can therefore be expected to reduce the evaporation rate by a factor of $[1\text{-}h_s/h_o]$ compared to a droplet of the same volume and contact angle (equal to the apparent contact angle) on a non-SLIPS surface.

An improved self-consistent model for evaporation of small sessile droplets was derived by Bourgès-Monnier and Shanahan[33] and is equivalent to,

$$f_{BMS}(\theta) = \frac{-\cos\theta}{2\log_e(1-\cos\theta)} \tag{9}$$

In the most recent work by Stauber *et al*.[9] on the evaporation of droplets on strongly hydrophobic substrates and which focused on the constant contact angle and constant contact radius modes, their formulae are equivalent to,

$$f_{SWDS}(\theta) = \frac{\sin\theta\, g(\theta)}{4(1+\cos\theta)^2} \tag{10}$$

where

$$\frac{g(\theta)}{(1+\cos\theta)^2} = \tan\left(\frac{\theta}{2}\right) + 8\int_0^\infty \frac{\cosh^2(\theta\tau)}{\sinh(2\pi\tau)} \tanh[\tau(\pi-\theta)]d\tau \tag{11}$$

Most importantly for analysing data, an exact solution for eq. (5) was derived by Picknett & Bexon[6] and they gave a numerically accurate polynomial interpolation for $f(\theta)$,

$$f_{PB}(\theta)=\begin{cases}\frac{1}{2}\left(0.6366\theta+0.09591\theta^2-0.06144\theta^3\right) & 0^0<\theta<10^0\\ \frac{1}{2}\left(0.00008957+0.6333\theta+0.116\theta^2-0.08878\theta^3+0.01033\theta^4\right) & 10^0<\theta<180^0\end{cases} \quad (12)$$

where $\theta$ in the series is in radians.

Following our earlier approach of using the apparent contact angle at the height $h_s$ of the lubricant skirt above the surface structure to define the droplet liquid-vapour interfacial area through which evaporation occurs, eq. (6) becomes,

$$\frac{dV}{dt}=-2\lambda R f(\theta_s) \quad (13)$$

Writing the spherical cap radius in terms of the drop volume and apparent contact angle $\theta_o$ at $z$=0, and then assuming both $\theta_o$ and $\theta_s$ are approximately constant allows the volume dependence on time to be found,

$$V(t)^{2/3}\approx V_i^{2/3}-\frac{4\lambda}{3}\left[\frac{3}{\pi\beta(\theta_o)}\right]^{1/3} f(\theta_s)\,t \quad (14)$$

where $V_i$ is the initial droplet volume at $t$=0. In terms of the apparent contact radius at $z$=0, this can be rewritten,

$$r_o^2\approx r_i^2-\frac{4\lambda t\sin^2\theta_o f(\theta_s)}{\pi\beta(\theta_o)}=r_i^2-\frac{2\lambda t\sin^2\theta_o}{\pi(1-\cos\theta_o)(2+\cos\theta_o)}\left(\frac{2f(\theta_s)}{1-\cos\theta_o}\right) \quad (15)$$

where $r_i$ is the initial apparent contact radius.

## 3. EXPERIMENTAL METHODS

### *3.1 SLIPS Surfaces*

For a lubricating liquid to spontaneously impregnate surface features, it is necessary that its contact angle in air on a chemically identical and smooth surface is below a critical angle defined as,

$$\cos\theta_c = \frac{1-\varphi_s}{r_w-\varphi_s} \tag{16}$$

where $\theta_c$ is the critical angle for hemi-wicking[34], $\varphi_s$ is the Cassie solid fraction of the projected area of the textured surface and $r_w$ is the Wenzel roughness defined as the ratio of its actual surface area to its projected area. The lubricating liquid, usually an oil, will impregnate the surface textures only if $\theta_{os(a)} < \theta_c$ where $\theta_{os(a)}$ is the contact angle of the lubricating liquid (*o*) on smooth solid (*s*) in the presence of air (*a*). Similarly, the condition for impregnation under water is $\theta_{os(w)} < \theta_c$, where $\theta_{os(w)}$ is the lubricant's contact angle on smooth solid in the presence of water (*w*). These possible thermodynamic states of a water droplet on an oil-infused surface have previously been described by Smith *et al*[26].

For this study the surface was chosen such that it could be accurately textured and easily functionalised chemically. We used silicon wafers, lithographically patterned using SU-8 photoresist and functionalised with octadecyltrichlorosilane (OTS) to add hydrophobicity. Studies[26, 27] have shown that silicone oil spreads on flat, smooth surfaces coated with OTS in the presence of both air and water ($\theta_{os(a)} = 0^o$ and $\theta_{os(w)} = 0^o$). This means that silicone oil will impregnate and flow atop surface features, but will be difficult to displace by water. By varying the roughness of the surface we hoped to achieve the ideal case for SLIPS surfaces. Figure 2a

shows a SEM image of a set of pillars of dimensions 50μm × 50μm cross section and a height of 50μm. Figure 2b shows a schematic of the production method and the expected impregnation regime for the SLIPS surface. Figure 2c shows an, SEM image taken with a back scatter detector in low vacuum mode, of the same substrate as Figure 2a, but impregnated with silicone oil to create the lubricating layer.

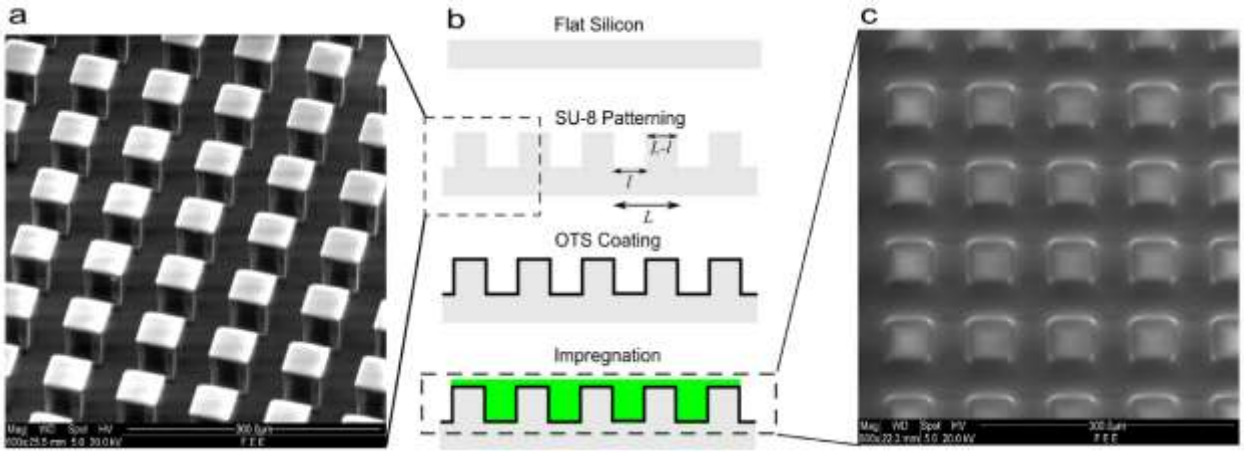


Figure 2: a) SEM image of a lithographically patterned SU-8 surface texture. b) Schematic showing the process to create the lubricated textured surfaces used in this study. c) SEM image showing the surface texture impregnated with the silicone oil lubricating liquid.

### *3.2 Fabrication of Textured Surfaces*

We constructed surfaces consisting of square pillars of SU-8 photoresist with pillar widths ranging from 10 μm to 90 μm arranged in square lattice patterns such that the centre-to-centre separation between pillars ($L$) is 100 μm. For example, a sample with 40 μm wide pillars ($L$-$l$) would give pillar separation ($l$) of 60 μm (Figure 2b). The two-dimensional Cassie surface area fraction, $\varphi_s = 1-(L-l)^2/L^2$, therefore ranged from 0.01 to 0.81. SU-8 is an epoxy based negative photoresist that can be spin coated or spread over a range of thicknesses to fabricate thick patterns with smooth walls using photolithography. The SU-8 becomes strong, stiff and

chemically resistant after processing and has a typical static water contact angle of $\theta \approx 80^{o}$ on a flat and smooth surface with large contact angle hysteresis[35]. Textured surfaces were created using 4" diameter polished silicon wafers (Pi-KEM). They were first cleaned with acetone and 2-propanol followed by a 10 minute bake at 100 °C to remove any remaining solvent. The substrate was then treated with an adhesion promoter (hexamethyldisilazane) prior to applying SU-8 2025 (MicroChem) resist. The amount of resist deposited onto each substrate was controlled at 4 ml. The spin coating consists of two stages. Substrates were first accelerated to 500 rpm at 164 rpm/s for 10 s and 1770 rpm at 328 rpm/s and for 30 s to achieve a required thickness of $h_p$=50µm. Since $L$ is kept at 100µm the Wenzel roughness, $r_w = 1+4h(L-l)/L^2$, for these samples therefore ranges from 1.2 to 2.8. The coated substrate was then baked on a hotplate for 3 min at 65 °C followed by 6 min at 95 °C. Substrates were then allowed to cool down to room temperature and the inner portion of the substrate was patterned to minimise thickness variation in the surface features due to edge defects. The SU-8 coated substrates underwent UV exposure in a mask aligner (EVG 620) under hard contact mode with an exposure dosage of 160 mJ/cm$^2$. Post-exposure baking was performed on a hotplate for 1 min at 65 °C followed by 6 min at 95 °C before being left to cool to room temperature. Following the post-exposure bake, the substrates were developed in EC solvent and agitated for 5 min in a sonicating bath. The developed substrate was washed with fresh EC solvent for approximately 10 s followed by rinse with 2-propanol before being dried using nitrogen gas. A final 15 min hard bake at 200 °C was added to ensure that the SU-8 photoresist properties did not change during use as a substrate for evaporation experiments.

### *3.3. Surface Chemistry Modification*

A hydrophobic coating was applied to the samples to prevent water from displacing the lubricating liquid and wetting the SU-8 features. Prior to impregnation they were cleaned once more with acetone and 2-propanol followed by a 10 minute bake at 100 °C to completely remove any remaining solvent. An OTS in hexane solution was prepared using 200 ml of hexane and 50µl of OTS. The solution was covered and then sonicated for 20 min. Meanwhile, samples were treated with oxygen plasma (Plasmalab 80Plus, Oxford Instruments) to promote adhesion of the OTS to the surface. The substrates were then placed in the Hexane/OTS mixture for 1 hour. After this time, samples were then extracted from the mixture and immediately placed in a fresh beaker of pure hexane and sonicated for a further 15 min prior to being baked on a hotplate for 15 min at 110°C.

### *3.4 Impregnation with Lubricating Liquid*

To create a uniform impregnation layer on the surfaces, the samples were dip coated in lubricating liquid to create the SLIPS surface and for this silicone oil (Sigma-Aldrich) was used. The textured surfaces were attached to glass slides and completely immersed in the oil. They were then vertically withdrawn from the liquid at a speed of 1 mm $s^{-1}$. This speed was found to be optimal according to the equation $V_{crit} = 0.12\mu_o\gamma_{LV}(\delta/\kappa^{-1})^{3/2}$, where $\mu_o$ is the viscosity of the lubricating liquid and $\delta$ is the height of the surface textures[36]. At this speed, a uniform coating and impregnation is achieved.

### *3.5 Determining the Drop Shape and Contact Angle*

Static contact angle measurements of water droplets on both textured (prior to lubrication) and flat substrates were carried out using a Krüss DSA30 Contact Angle meter. Dynamic contact angle measurements were also carried out to determine the contact angle hysteresis by

calculating the difference between the advancing and receding contact angles. The contact angle hysteresis for the samples was also determined by measuring the sliding angle of water droplets using the tilt table on the Krüss Contact Angle meter.

For droplets on the lubricated textured surfaces, the majority of the profiles conformed to a circular arc, consistent with expectations for droplets of sizes less than the capillary length. We therefore extracted data points on the outer edge of the droplet and fitted a circular arc using a bespoke MATLAB® program (a representative selection of points is shown in Figure 3 as an example). To obtain the apparent contact angles defined in Figure 1b, we fitted baselines at the base of the droplet and the wetting ridge, and at the top of the wetting ridge and used their intersection with the circular arc. The top of the wetting ridge was determined by sampling the data points from the profile close to the substrate that lie on the wetting ridge-vapour interface and finding the point of inflection of the profile given by the data points.

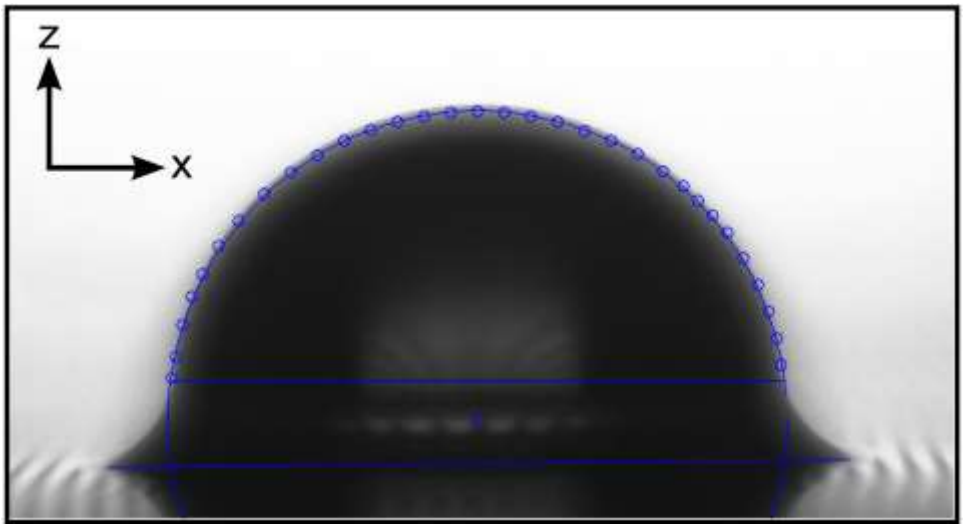


Figure 3: Image of a droplet on a lubricated textured surface with a sample of extracted data points on the side view profile of the spherical cap surface.

### *3.6 Droplet Evaporation Experiments*

Small droplets of water (2.5 ± 0.2 μl) were deposited using a Proline Plus 2-25 μl pipette on each surface. These were allowed to evaporate in a monitored enclosed environment, and images of the droplets were taken at 30 second intervals for a maximum of 2500 seconds. All experiments in this study were carried out at room temperature (20-25 °C) and constant relative humidity (25-35%) in a bespoke environmental chamber to minimise humidity variations and protect from air currents within the laboratory. A temperature and humidity sensor (DHT22, Aosong Electronics) was placed inside of the chamber and connected to a LabVIEW™ program via an Arduino microcontroller. The LabVIEW program was used to image the droplet at the specified time-lapse interval and stamp the images with the time, date, temperature and relative humidity ready for post-experiment analysis. Apparent contact angles and contact base diameter were obtained from the images and the liquid-vapour surface area, spherical radius and hydrostatic pressure (using the young Laplace equation) as a function of time was calculated. To check reproducibility, three separate evaporation experiments were performed on each sample, these showed a variation of < 4% in apparent contact radius at each time interval, and the average values of the aforementioned measurements were used in the analysis process. Axial symmetry was assumed in the evaporation process and used in image processing calculations[17]. The assumption of axial symmetry is very strongly obeyed for a SLIPS surface where water droplets sit on top of a lubricating liquid in contrast to the case of direct liquid droplet-solid substrate contact which can involve contact line pinning. This was confirmed in this case with top view imaging of the droplet and image processing.

## 4. RESULTS AND DISCUSSION

### *4.1 Sliding Angles*

Figure 4 shows images of droplets when placed on the different lubricated textured surfaces. In all cases the major part of the profile follows a spherical cap shape, but with a small wetting ridge. To test the effectiveness of the lubricated textured surfaces as SLIPS surfaces in supporting mobile droplets, 1mm diameter droplets of water were placed on each surface and the sliding angle was measured (

**Table 1**). Here we use the linear lubricant fraction, $l_f = l/L$, as a naming convention for samples. The sliding angle for all of the nine sample designs, with $l_f$ = 0.1, 0.2, 0.3, 0.4, 0.5, 0.6, 0.7, 0.8, 0.9, was very low (typically ~1° with some achieving as low as 0.3°) with very low contact angle hysteresis. We consider these as ideal SLIPS surfaces with highly mobile contact lines. However, some of the fabricated samples did not show the same low hysteresis characteristics and where therefore classified as non-SLIPS surfaces. For example, in one batch of surfaces, for three of the samples with $l_f$ =0.1, 0.4, 0.6, the sliding angle were much higher, $25.3^o \pm 0.6^o$, $29.8^o \pm 4.7^o$, and$16.6^o \pm 3.5^o$, respectively. This discrepancy may be due to the failure of the OTS functionalization process, which is more difficult to achieve on an SU-8 surface than surfaces such as silicon and glass.

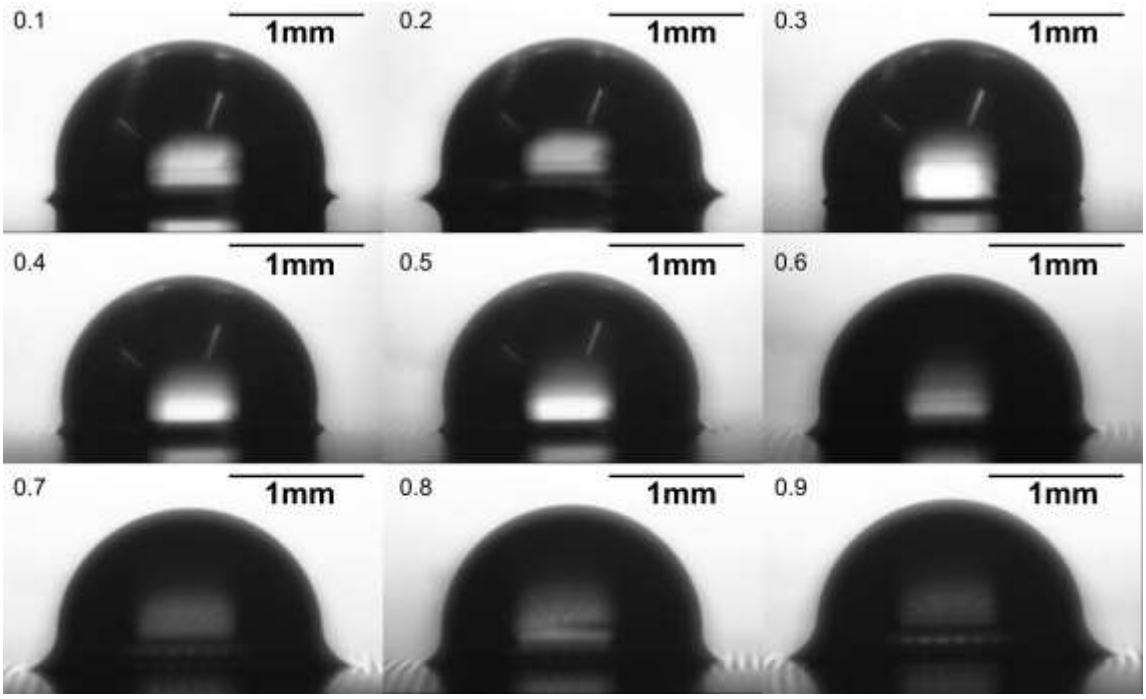


Figure 4: Water droplets on surfaces with different lubricated surface textures: $l_f$=0.1 – 0.9 indicates the ratio of texture gap width to unit length which in this study has been set as 100 μm.

Table 1: The sliding angle of water droplets for surfaces with different linear lubricant fraction, $l_f$, and low sliding angle

| **Linear lubricant fraction, $l_f$** | **0.1** | **0.2** | **0.3** | **0.4** | **0.5** | **0.6** | **0.7** | **0.8** | **0.9** |
|---|---|---|---|---|---|---|---|---|---|
| **Cassie fraction, $\varphi_s$** | 0.81 | 0.64 | 0.49 | 0.36 | 0.25 | 0.16 | 0.09 | 0.04 | 0.01 |
| **Wenzel roughness, $r_w$** | 2.8 | 2.6 | 2.4 | 2.2 | 2 | 1.8 | 1.6 | 1.4 | 1.2 |
| **Sliding angle(°)** | 0.9 ±0.1 | 1.3 ±0.1 | 0.6 ±0.1 | 0.7 ±0.1 | 0.7 ±0.1 | 0.3 ±0.1 | 0.3 ±0.1 | 0.4 ±0.1 | 0.5 ±0.1 |

### *4.2 Constant Contact Angle Mode Evaporation*

On surfaces with low sliding angles, and therefore classified as SLIPS, the evaporation of a water droplet proceeds with a steadily decreasing droplet volume and apparent contact area. A wetting ridge is observed close to the substrate and visually the apparent contact angle, defined by the intersection of the spherical cap droplet profile and the baseline, appears to be above $90^{o}$ and constant during evaporation as shown by the representative example time series of image in Figure 5.

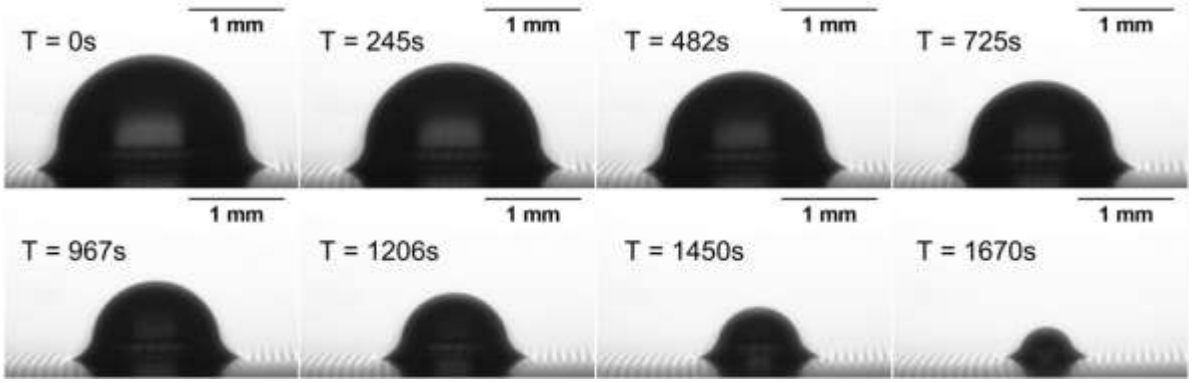


Figure 5: Images of a typical droplet evaporating on a low sliding angle SLIPS surface.

Figure 6 shows the time dependence of the square of the apparent contact radius $r_0^2$ for the samples classified as SLIPS surfaces using the criteria of low sliding angle values. The high mobility and low hysteresis of the apparent contact line provide a linear relationship from the very start of the evaporation process. This data shows a strong linear relationship over the entire range of the evaporation process and provides further confidence, in addition to the observed constancy of the apparent contact angle, that within the context of the diffusion limited evaporation model the droplet is undergoing constant contact angle evaporation.

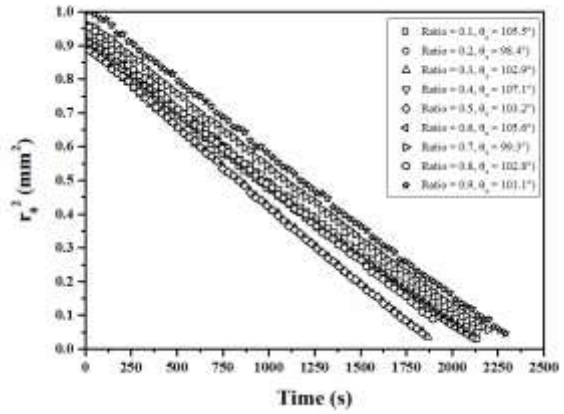


Figure 6: Linearity of $r_0^2$ during the evaporation of the samples with spacing/unit length ratio $l_f$= 0.1 – 0.9.

To test the validity of equation 15 and to provide further confidence in the $r_0^2$ versus time relationship we estimated the diffusion coefficients of the droplets from the gradients, $m$, of the data in Figure 6, i.e.

$$D = \frac{m\rho(1-\cos\theta_o)(2+\cos\theta_o)}{4(c_s - c_\infty)\sin^2\theta_o}\left(\frac{1-\cos\theta_o}{2f_{PB}(\theta_s)}\right) \qquad (17)$$

Experimentally the two apparent contact angles, $\theta_o$ and $\theta_s$, are observed to remain constant throughout the evaporation process. We assume complete saturation of the air at the droplet liquid/vapour interface and calculate the value of $c_\infty$ using the relationship:

$$\text{Relative Humidity} = \frac{\text{Actual vapour density}}{\text{Saturation vapour density}} \times 100\% \qquad (18)$$

where $c_\infty$ is the actual vapour density and the value of $c_s$ was obtained from reference data[37] for different temperatures. For example, for the droplet evaporation on a sample with the ratio $l_f$ = 0.9, the slope is $(4.282 \pm 0.012)\times10^{-4}$ mm$^2$ s$^{-1}$, $\theta_o = 101.1 \pm 1.0^o$ and $\theta_s = 84.4 \pm 1.0^o$. The humidity of 38.4% and temperature of 23.3°C gives $(c_s\text{-}c_\infty)=(12.66 \pm 0.10) \times 10^{-3}$ gm$^{-3}$. Therefore the

diffusion coefficient calculated from these values is $D=(2.39 \pm 0.20)\times10^{-5}\,m^2\,s^{-1}$. This compares favourably (to within 2%) with the value of $D=2.43 \times 10^{-5}\,m^2\,s^{-1}$ calculated from a linear fit to reference data obtained from the CRC Handbook[38] for diffusion of water vapour into air. Table 2 shows the calculated values of the diffusion coefficient, *D*, for all droplets on surfaces classified as SLIPS surfaces by low values of sliding angles. They show an excellent correlation, within an average difference of 4% with the literature values.

Table 2: Estimates of diffusion coefficients for water into air for droplets on SLIPS surfaces.

| **Ratio $l_f$** | **RH (%)** | **$T$ (°C)** | **$\Delta c$ (g m$^{-3}$)** | **$\theta_o$ (°)** | **$\theta_s$ (°)** | **$h_s/h_{o(i)}$ (%)** | **$D$ (×10$^{-5}$ m$^2$ s$^{-1}$)** | **$D_o$ (×10$^{-5}$ m$^2$ s$^{-1}$)** | **$D_o/D$ (%)** | **$D$ (Lit) (×10$^{-5}$ m$^2$ s$^{-1}$)** |
|---|---|---|---|---|---|---|---|---|---|---|
| 0.1 | 48.3 | 26.2 | 13.16 | 105.5 | 86.5 | 13.7 | 2.44 ± 0.19 | 2.10 ± 0.19 | 86 | 2.50 |
| 0.2 | 34.0 | 22.2 | 12.81 | 98.4 | 90.5 | 13.4 | 2.13 ± 0.18 | 1.96 ± 0.16 | 92 | 2.41 |
| 0.3 | 34.2 | 22.2 | 12.76 | 102.9 | 97.6 | 6.7 | 2.42 ± 0.20 | 2.26 ± 0.19 | 93 | 2.41 |
| 0.4 | 47.2 | 26.4 | 13.59 | 107.1 | 87.3 | 16.7 | 2.46 ± 0.19 | 2.11 ± 0.19 | 86 | 2.50 |
| 0.5 | 34.2 | 22.5 | 12.76 | 103.2 | 94.7 | 8.5 | 2.50 ± 0.21 | 2.28 ± 0.19 | 91 | 2.41 |
| 0.6 | 46.9 | 26.7 | 13.91 | 105.6 | 88.3 | 13.1 | 2.36 ± 0.18 | 2.07 ± 0.18 | 88 | 2.52 |
| 0.7 | 38.0 | 22.8 | 12.74 | 99.3 | 87.0 | 19.3 | 2.21 ± 0.18 | 1.96 ± 0.16 | 89 | 2.43 |
| 0.8 | 37.9 | 23.3 | 12.76 | 102.8 | 90.6 | 13.6 | 2.50 ± 0.21 | 2.21 ± 0.18 | 88 | 2.43 |
| 0.9 | 38.4 | 23.3 | 12.66 | 101.1 | 84.4 | 20.5 | 2.39 ± 0.20 | 2.03 ± 0.17 | 85 | 2.43 |

It is possible to quantify the order of magnitude of the effect of the wetting skirt on estimates of the diffusion constant *D*, by using $\theta_o$ instead of $\theta_s$ in $f_{PB}(\theta)$ in eq. (17). These estimates are shown as $D_o$ in Table 2 and these are systematically lower than the estimates of *D*. On average these estimates across all samples would have had a 14% difference from the literature values compared to an average difference of 4% when using the model with the wetting skirt. To further test the effect of the wetting skirt on diffusion limited evaporation would require SLIPS surfaces with lower apparent contact angles and higher wetting skirts as a proportion of the initial droplet apex height , $h_{o(i)}$.

Another possible limitation on the estimates of the diffusion constant is the assumption that evaporation proceeds across a water-air interface. Smith *et al.* have previously noted that a lubricating liquid impregnated into a SLIPS surface may spread and cloak the droplet with a thin layer, possibly a monolayer, of the lubricating liquid[26]. If this were to occur, the evaporation would proceed through a combined water-oil-air interface and this could reduce the evaporation rate. To spread over and cloak the droplet, the spreading coefficient of the lubricating liqud, *S*, on water (*w*) in the presence of air (*a*), $S_{ow}(a)= \gamma_{wa}-\gamma_{ow}-\gamma_{oa}$, has to be greater than zero, whereas $S_{ow}(a) < 0$ implies the oil will not cloak the droplet. Using the value of $\gamma_{ow}$ obtained from literature[39] and the value of $\gamma_{oa}$ provided by Dow Corning for the silicone oil gives $S_{ow}(a)$ = 5.1 mN/m. This implies that the oil should cloak the droplet, although we did not observe such an effect. In our analysis we assume the layer of oil either does not cloak the droplet or is sufficiently thin for its effect on the evaporation rate to be negligible.

### *4.3 Mixed Mode Evaporation*

In the mixed mode of evaporation changes in both the contact area (equivalently the contact radius) and contact angle occur. Figure 7 shows an example of a droplet evaporating on a lubricated textured non-SLIPS surface classified as such according to having a high sliding angle. Under these lighting conditions the underlying texture of the surface is almost visible, but the constant contact angle mode evaporation was not observed for extended times on these samples deemed to be non-SLIPS surfaces according to the sliding angle criteria. There was, however, a brief initial stage during the evaporation process that showed approximately constant contact angle evaporation. The droplet appeared to initially evaporate with a constant apparent contact angle $\theta_o$ and a diminishing apparent contact radius. The contact line then appeared to pin and $\theta_o$

began to drop. Interestingly, the contact line subsequently appeared to de-pin and show a contraction in apparent contact radius before becoming pinned once again. This stick-slip process repeated itself throughout the remainder of the evaporation process.

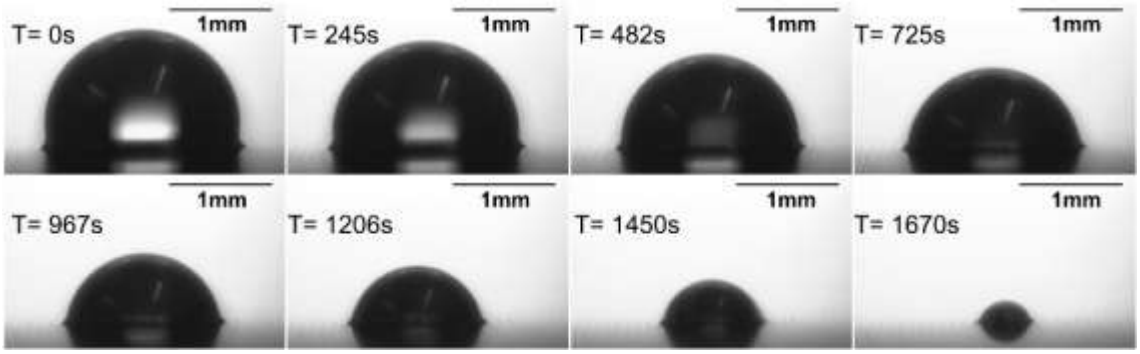


Figure 7: Images of a typical droplet evaporating on a non-SLIPS surface.

Figure 8 shows example data for a droplet on one of the non-SLIPS surface and clearly shows stepping, which is characteristic of a stick-slip regime[40, 41]. Figure 9 shows a plot of a portion of the time sequence data for the lubricated texture with $l_f$ = 0.4 and a sliding angle of 29.8°±4.7°, where this stepping is highly prevalent. The steps in the data appear to rapidly change the contact radius by approximately 35 μm. This value corresponds approximately to the value for the gaps between pillars of 40 μm for this texture's value of linear lubricant fraction. When a drop in apparent contact radius occurs an increase in the contact angle, $\theta_o$ is also observed. $\theta_o$ decreases as the contact line is pinned and increases as the contact line de-pins (Figure 9).

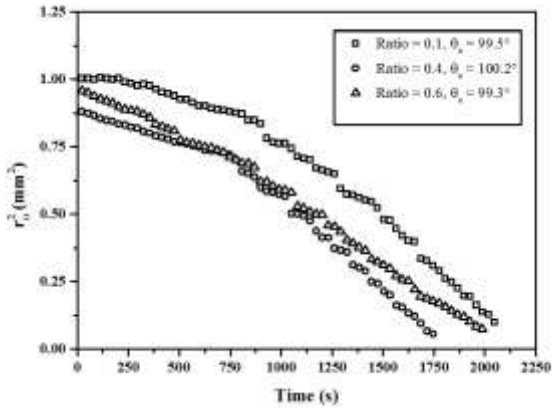


Figure 8: Plot of the square of drop apparent contact radius as a function of time for sessile droplet evaporation on a non-SLIPS surface.

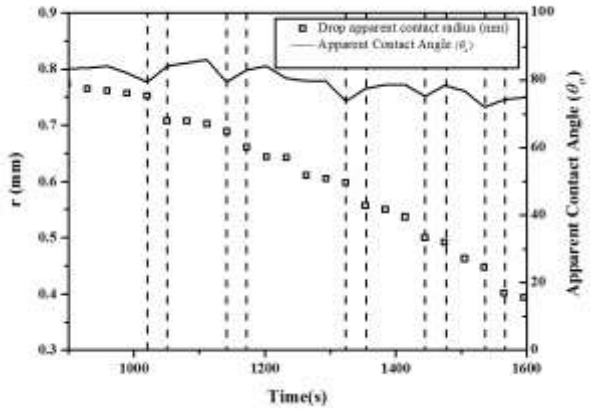


Figure 9: Plot of drop apparent contact radius and apparent contact angle as a function of time for non-SLIPS sample with $l_f$=0.4 where the width of pillars is 60μm and the gap between pillars is 40μm and a sliding angle of $29.8^o \pm 4.7^o$. The sudden changes in drop apparent contact radius roughly correspond to spacing of 40μm as the contact line jumps across pillar gaps. Vertical dashed lines indicate increases in apparent contact angle where a sudden drop in apparent contact radius occurs.

Although non-SLIPS samples did not exhibit constant contact angle evaporation throughout the entirety of the experiments, it is interesting to note that a brief constant contact angle period was observed in the initial stage before showing a stepwise retreat. It is therefore possible that, due to variations in the quality of the OTS coating, these surfaces were initially very close to

becoming SLIPS surfaces and the increase in the Laplace pressure as the droplet evaporated may have forced the water in the droplet into direct contact with the solid surface at the top of the pillars. This would represent a transition from a true SLIPS state to a hemi-wicked Cassie-Baxter type state where the droplet rests on a combination of the solid tops of pillars and the oil-filled gaps between pillars. This transition to a more sticky state would be analogous to what has been observed to occur on a superhydrophobic surface when an evaporating drop undergoes a transition from a Cassie-Baxter state to a Wenzel state. In the SLIPS case a further transition to a Wenzel state whereby the water fully displaces oil within the gaps of the texture might also be possible, although this would require substantial reductions on droplet curvature to generate excess Laplace pressure. An interpretation of water displacement of oil from the tops of pillars, if substantiated, would suggest that the tilt angle method of making a sliding angle measurement might also cause a slippery to sticky transition in some samples.

## 5. CONCLUSION

The diffusion-limited evaporation of small droplets of water placed on lubricated textured surfaces, classified as Slippery Liquid-Infused Porous Surfaces (SLIPS) by their low sliding angles, has been studied. This type of surface allows for high apparent contact angle (~100°) droplets, and gives a highly mobile apparent contact line which allows a constant contact angle mode type of evaporation. The presence of a wetting ridge created by the balance of the three interfacial forces at the line of contact between the droplet, the infusing liquid at the base of the droplet and air (often represented by a Neumann triangle) has been accounted for by extrapolating an apparent contact angle with the surface. A model has been developed which accounts for the wetting ridge by the concept of a wetting skirt limiting the droplet liquid-vapour

surface area available for the evaporation. This model provides a linear dependence of the apparent contact surface area on time. On surfaces which showed ideal low sliding angle SLIPS characteristics this model has allowed us to calculate the diffusion coefficients for water in air and excellent correlation, to within an average of 4% of reference values was obtained. On lubricated textured surfaces which did not show ideal low sliding angle SLIPS characteristics the droplets did not demonstrate constant contact angle evaporation during extended times. They did, however, show evidence of the droplet transitioning into a stick-slip regime. The size of the stick-slip jumps of the apparent contact radius data was 35 μm which approximately corresponds to the surface texture spacing. This transition is possibly due to droplets transitioning from an ideal SLIPS state to one with direct droplet contact with the tops of pillars or to an oil hemi-wicked Cassie-Baxter state under increased excess Laplace pressure as their spherical radius of curvature reduces, displacing the lubricating liquid and coming into contact with the surface texture.

## AUTHOR INFORMATION

### Corresponding Author

*E-mail: gary.wells@northumbria.ac.uk

#### Notes

The authors declare no competing financial interest.

## ACKNOWLEDGMENTS

J.H.G gratefully acknowledges financial support from Reece Innovation and the University of Northumbria at Newcastle *via* a postgraduate research studentship. The authors also acknowledge Dr Linzi E. Dodd, Dr Michael Cooke and Dr Pietro Maiello for valuable advice and technical support.

**REFERENCES**


1. Erbil, H. Y. Evaporation of Pure Liquid Sessile and Spherical Suspended Drops: A Review. *Adv. Colloid Interface Sci.* **2012,** *170* (1–2), 67-86.

2. Park, J.; Moon, J. Control of Colloidal Particle Deposit Patterns within Picoliter Droplets Ejected by Ink-Jet Printing. *Langmuir* **2006,** *22* (8), 3506-3513.

3. Kimura, M.; Misner, M. J.; Xu, T.; Kim, S. H.; Russell, T. P. Long-Range Ordering of Diblock Copolymers Induced by Droplet Pinning. *Langmuir* **2003,** *19* (23), 9910-9913.

4. Jing, J.; Reed, J.; Huang, J.; Hu, X.; Clarke, V.; Edington, J.; Housman, D.; Anantharaman, T. S.; Huff, E. J.; Mishra, B.; Porter, B.; Shenker, A.; Wolfson, E.; Hiort, C.; Kantor, R.; Aston, C.; Schwartz, D. C. Automated High Resolution Optical Mapping using Arrayed, Fluid-Fixed DNA Molecules. *Proc. Natl. Acad. Sci. USA* **1998,** *95* (14), 8046-8051.

5. Yu, Y.; Zhu, H.; Frantz, J. M.; Reding, M. E.; Chan, K. C.; Ozkan, H. E. Evaporation and Coverage Area of Pesticide Droplets on Hairy and Waxy Leaves. *Biosystems Engineering* **2009,** *104* (3), 324-334.

6. Picknett, R., G; Bexon, R. The Evaporation of Sessile or Pendent Drops in Still Air. *J. Colloid Interf. Sci* **1977,** *61*, 366-350.

7. Cazabat, A.-M.; Guena, G. Evaporation of Macroscopic Sessile Droplets. *Soft Matter* **2010,** *6* (12), 2591-2612.

8. Larson, R. G. Transport and Deposition Patterns in Drying Sessile Droplets. *AIChE Journal* **2014,** *60* (5), 1538-1571.

9. Stauber, J. M.; Wilson, S. K.; Duffy, B. R.; Sefiane, K. Evaporation of Droplets on Strongly Hydrophobic Substrates. *Langmuir* **2015,** *31* (12), 3653-3660.

10. Birdi, K. S.; Vu, D. T.; Winter, A. A Study of the Evaporation Rates of Small Water Drops Placed on a Solid Surface. *J. Phys. Chem.* **1989,** *93* (9), 3702-3703.

11. Birdi, K. S.; Vu, D. T. Wettability and the Evaporation Rates of Fluids from Solid Surfaces. *J. Adhes. Sci. Technol.* **1993,** *7* (6), 485-493.

12. Shanahan, M. E. R.; Bourgès, C. Effects of Evaporation on Contact Angles on Polymer Surfaces. *Int. J. Adhes. Adhes.* **1994,** *14* (3), 201-205.

13. Rowan, S. M.; Newton, M. I.; McHale, G. Evaporation of Microdroplets and the Wetting of Solid Surfaces. *J. Phys. Chem.* **1995,** *99* (35), 13268-13271.

14. Rowan, S. M.; McHale, G.; Newton, M. I.; Toorneman, M. Evaporation of Microdroplets of Three Alcohols. *J. Phys. Chem. B* **1997,** *101* (8), 1265-1267.

15. McHale, G.; Rowan, S. M.; Newton, M. I.; Banerjee, M. K. Evaporation and the Wetting of a Low-Energy Solid Surface. *J. Phys. Chem. B* **1998,** *102* (11), 1964-1967.

16. Cassie, A. B. D.; Baxter, S. Wettability of Porous Surfaces. *Trans. Faraday Soc.* **1944,** *40* (0), 546-551.

17. McHale, G.; Aqil, S.; Shirtcliffe, N. J.; Newton, M. I.; Erbil, H. Y. Analysis of Droplet Evaporation on a Superhydrophobic Surface. *Langmuir* **2005,** *21* (24), 11053-11060.

18. Wenzel, R. N. Resistance of Solid Surfaces to Wetting by Water. *Ind. Eng. Chem.* **1936,** *28* (8), 988-994.

19. Tsai, P.; Lammertink, R. G. H.; Wessling, M.; Lohse, D. Evaporation-Triggered Wetting Transition for Water Droplets upon Hydrophobic Microstructures. *Phys. Rev. Lett.* **2010,** *104* (11), 116102.

20. Gelderblom, H.; Marín, Á. G.; Nair, H.; van Houselt, A.; Lefferts, L.; Snoeijer, J. H.; Lohse, D. How Water Droplets Evaporate on a Superhydrophobic Substrate. *Phys. Rev. E* **2011,** *83* (2), 026306.

21. Jung, Y. C.; Bhushan, B. Wetting Behaviour during Evaporation and Condensation of Water Microdroplets on Superhydrophobic Patterned Surfaces. *Journal of Microscopy* **2008,** *229* (1), 127-140.

22. Tan, S.-x.; Zhang, X.-y.; Zhao, N.; Xu, J. Simulation of Sessile Water-Droplet Evaporation on Superhydrophobic Polymer Surfaces. *Chin. J. Chem. Phys.* **2007,** *20* (2), 140.

23. Zhang, X.; Tan, S.; Zhao, N.; Guo, X.; Zhang, X.; Zhang, Y.; Xu, J. Evaporation of Sessile Water Droplets on Superhydrophobic Natural Lotus and Biomimetic Polymer Surfaces. *ChemPhysChem* **2006,** *7* (10), 2067-2070.

24. Kulinich, S. A.; Farzaneh, M. Effect of Contact Angle Hysteresis on Water Droplet Evaporation from Super-Hydrophobic Surfaces. *Appl. Surf. Sci.* **2009,** *255* (7), 4056-4060.

25. Quéré, D. Non-Sticking Drops. *Rep. Prog. Phys.* **2005,** *68* (11), 2495.

26. Smith, J. D.; Dhiman, R.; Anand, S.; Reza-Garduno, E.; Cohen, R. E.; McKinley, G. H.; Varanasi, K. K. Droplet Mobility on Lubricant-Impregnated Surfaces. *Soft Matter* **2013,** *9* (6), 1772-1780.

27. Solomon, B. R.; Khalil, K. S.; Varanasi, K. K. Drag Reduction using Lubricant-Impregnated Surfaces in Viscous Laminar Flow. *Langmuir* **2014,** *30* (36), 10970-6.

28. Wong, T.-S.; Kang, S. H.; Tang, S. K. Y.; Smythe, E. J.; Hatton, B. D.; Grinthal, A.; Aizenberg, J. Bioinspired Self-Repairing Slippery Surfaces with Pressure-Stable Omniphobicity. *Nature* **2011,** *477* (7365), 443-447.

29. Huang, X.; Chrisman, J. D.; Zacharia, N. S. Omniphobic Slippery Coatings Based on Lubricant-Infused Porous Polyelectrolyte Multilayers. *ACS Macro Lett.* **2013,** *2* (9), 826-829.

30. Manna, U.; Lynn, D. M. Fabrication of Liquid-Infused Surfaces Using Reactive Polymer Multilayers: Principles for Manipulating the Behaviors and Mobilities of Aqueous Fluids on Slippery Liquid Interfaces. *Adv. Mater.* **2015,** *27* (19), 3007-3012.

31. Kim, P.; Wong, T.-S.; Alvarenga, J.; Kreder, M. J.; Adorno-Martinez, W. E.; Aizenberg, J. Liquid-Infused Nanostructured Surfaces with Extreme Anti-Ice and Anti-Frost Performance. *ACS Nano* **2012,** *6* (8), 6569-6577.

32. Erbil, H. Y.; McHale, G.; Newton, M. I. Drop Evaporation on Solid Surfaces: Constant Contact Angle Mode. *Langmuir* **2002,** *18* (7), 2636-2641.

33. Bourges-Monnier, C.; Shanahan, M. E. R. Influence of Evaporation on Contact Angle. *Langmuir* **1995,** *11* (7), 2820-2829.

34. Bico, J.; Thiele, U.; Quere, D. Wetting of Textured Surfaces. *Colloids Surf., A* **2002,** *206* (1-3), 41-46.

35. Shirtcliffe, N. J.; Aqil, S.; Evans, C.; McHale, G.; Newton, M. I.; Perry, C. C.; Roach, P. The use of High Aspect Ratio Photoresist (SU-8) for Super-Hydrophobic Pattern Prototyping. *J. Micromech. Microeng.* **2004,** *14* (10), 1384.

36. Seiwert, J.; Clanet, C.; Quéré, D. Coating of a Textured Solid. *J. Fluid Mech.* **2011,** *669*, 55-63.

37. Kaye, G. W. C.; Laby, T. H. *Kaye & Laby Tables of Physical & Chemical Constants*; National Physical Laboratory2005.

38. Weast, R. C.; Astle, M.; Beyer, W. 1985: CRC Handbook of Chemistry and Physics. CRC Press, Inc., Boca Raton, FL, 1984.

39. Wang, C. Y.; Calabrese, R. V. Drop Breakup in Turbulent Stirred-Tank Contactors. Part II: Relative Influence of Viscosity and Interfacial Tension. *AIChE Journal* **1986,** *32* (4), 667-676.

40. Anantharaju, N.; Panchagnula, M.; Neti, S. Evaporating Drops on Patterned Surfaces: Transition from Pinned to Moving Triple Line. *J. Colloid Interface Sci.* **2009,** *337* (1), 176-182.

41. Orejon, D.; Sefiane, K.; Shanahan, M. E. R. Stick–Slip of Evaporating Droplets: Substrate Hydrophobicity and Nanoparticle Concentration. *Langmuir* **2011,** *27* (21), 12834-12843.

For table of contents only: